# Goldsmiths Research Online

*Goldsmiths Research Online (GRO)*
*is the institutional research repository for*
*Goldsmiths, University of London*

## Citation

## Persistent URL

## Versions

## Goldsmiths
### UNIVERSITY OF LONDON

# Abstract Shape Synthesis From Linear Combinations of Clelia Curves

L. Putnam, S. Todd and W. Latham

Computing, Goldsmiths, University of London, United Kingdom

**Abstract**

*This article outlines several families of shapes that can be produced from a linear combination of Clelia curves. We present parameters required to generate a single curve that traces out a large variety of shapes with controllable axial symmetries. Several families of shapes emerge from the equation that provide a productive means by which to explore the parameter space. The mathematics involves only arithmetic and trigonometry making it accessible to those with only the most basic mathematical background. We outline formulas for producing basic shapes, such as cones, cylinders, and tori, as well as more complex families of shapes having non-trivial symmetries. This work is of interest to computational artists and designers as the curves can be constrained to exhibit specific types of shape motifs while still permitting a liberal amount of room for exploring variations on those shapes.*

**CCS Concepts**
• *Computing methodologies* → *Parametric curve and surface models;* • *Applied computing* → *Media arts;*

## 1. Introduction

There is a large repertoire of mathematical systems and algorithms capable of generating rich and complex non-figurative graphics [Whi80, GBKW09, Ad80, Man82, PL90, TL92, Kaw82, Gie03, Wol02]. While in general having so many options available could be argued to be a good thing, from an artist's perspective this can be counterproductive as a disproportionate amount of time may be spent in searching for interesting output. Ideally, one would have a handful of constrained, yet highly productive 'veins' within a given shape generation algorithm to provide a starting point for both manual exploration and automated stochastic generation. The program of *generative mathematics* defined as "the study of mathematical operations suitable for generating artistic images" [Fra89] suggests an initial step towards attaining this goal.

Our interest in curve generating systems is motivated by the desire to use a singular yet polymorphic material in synthesizing abstract visual forms. In one sense this is a self-imposed artistic constraint, however it also provides a sense of cohesion and logic to the completed work. Additionally, it is important for us that the material is inherently *generative* acting as a creative partner with its own degree of processual autonomy [MBD*14]. Shape generation systems based on principles of repetition and recursion such as turtle graphics [Pap72, Ad80], L-systems [PL90], and vector-controlled shape synthesis [Gla97] are powerful, yet divert attention towards systems building. Other approaches such as the GROWTH model [Kaw82], harmonograms [Bro07] and meander curves [Cha15, Gai05] edge closer to balancing constraint and freedom.

We draw inspiration from specific artistic works such as Ernst Haeckel's illustrations of microscopic forms [BEEH98], M. C. Escher's curve-based sketches *Bond of Union*, *Spherical Spirals*, and *Concentric Rinds*, Naum Gabo's *Linear Construction* works, the oscillographic art of Ben Laposky [Lap53, Lap69] and Herbert Franke [Fra76], John Whitney's digital harmony [Whi80], and Todd and Latham's *FormGrow* virtual sculptures [TL92]. Related generative works include *Backscatter* (2005) by Robin Fox, *Embryo* (1988) by Yoichiro Kawaguchi, Jon McCormack's virtual plants in *Morphogenesis Series* (2001-2004) and *Bloom* (2006) [MBDJ04] and *Particle Dreams* (1988) by Karl Sims. The notion of using a single curve to generate patterns dates further back to art forms such as meander patterns, sona designs, Kolam drawings, Vanuata sand drawings, and Celtic knotwork. From a technological standpoint, the shapes are most closely linked to the intricate unicursal patterns produced by the geometric chuck [Baz75, ID33] and other automatic drawing machines [Rig26, GBKW09]. Figures produced from these drawing machines, including the chronophotographic experiments of Étienne-Jules Marey [Mar74, Mar95] and later oscillographic and computational systems, are a record of the motion of a point or other object and thus a translation of time into space.

The remaining sections detail our curve generation algorithm. Section 2 discusses general properties of the Clelia curve, used as

a building block to construct more complex curves, and Section 3 linear combinations of Clelia curves. Sections 4-10 present particular families (veins) of shapes produced from sums of Clelia curves. Compared to direct manipulation of the fundamental Clelia parameters, these families allow far more control over the structure of the resulting shape including its symmetries, density and overall envelope shape. Section 12 presents strategies for rendering the curves that enhance visual richness and examples of the artistic potential of the curve generation algorithm. We will not include a dedicated section on animation but note that good results are obtained by applying time-varying functions to the amplitude and phase values. Section 13 briefly describes the possibility of generating unified spatiotemporal forms.

## 2. Clelia Curve

Our fundamental building block is a sinusoidal curve lying on the surface of a sphere known as a Clelia curve. The Clelia curve was first studied by the Italian mathematician Guido Grandi and presented, along with the closely-related rose curve, in his work on 'geometric flowers' [Gra28]. Grandi named the Clelia curve after the Italian mathematician Clelia Grillo Borromeo. Mathematically, a Clelia may be defined as a curve that has linear dependent spherical coordinates [GdW16]. A Clelia curve may be produced as the path traced out by a point attached to a two-axis gimbal where the pivot axes are orthogonal and each ring spins with uniform angular velocity. Clelia curves may be generated digitally by a 3D turtle [Ad80] or through the FormGrow [TL92] commands *bend* and *twist*.

We chose the Clelia curve as a primitive as it satisfies several criteria important to us: 1) has well-defined bounds, 2) naturally creates closed surfaces, 3) has a high degree of symmetry, 4) is describable by a finite Fourier series and 5) is straightforward to implement. Being described by a finite Fourier series, one can obtain exact derivatives out to any order; this applies to linear combinations as well. Arguably, the simplest primitive might be three independent sinusoids along each dimension producing a 3D Lissajous curve [Lis57]. However, curves produced in this way naturally have a box-like appearance as with sound embedding [Wag70, MP98]. Under specific constraints, it is possible to create an "extruded" Lissajous curve that is a Lissajous figure when projected on one of the basis planes and oscillates sinusoidally along the axis orthogonal to the projection plane. The most symmetric of these particular shapes is a cylindrical sinusoid. Using a base curve with more intrinsic rotations [Put14] satisfies many of our criteria and may lead to a wider array of shapes, however, analysis becomes more involved. Similarly, a spherical product of two planar curves [GBB03] makes analysis more difficult and requires more parameters in describing each of the two curves.

### 2.1. Mathematical Description

This section outlines some basic definitions and properties of a Clelia curve that will be referenced in the remaining sections. We define a Clelia curve as

$$Cl_{G,\gamma,F,\beta}(t) = \begin{bmatrix} \cos(2\pi[Gt+\gamma])\sin(2\pi[Ft+\beta]) \\ \sin(2\pi[Gt+\gamma])\sin(2\pi[Ft+\beta]) \\ \cos(2\pi[Ft+\beta]) \end{bmatrix} \quad (1)$$

where $t \in [0,1)$ is a fraction of the curve period, $G$ and $F$ are frequencies in cycles/period and $\gamma$ and $\beta$ are phases in cycles. The frequencies $G$ and $F$ produce uniform angular motion along lines of latitude and longitude, respectively. The curve repeats $\gcd(F,G)$ times; to avoid this one must ensure that $F$ and $G$ are coprime. To clarify coprimality, we define the special values $F' = F/\gcd(F,G)$ and $G' = G/\gcd(F,G)$. For convenience, we define the shorthand forms

$$Cl_{G,\gamma,F,\beta}(t) = \{G,\gamma\}\{F,\beta\}$$
$$Cl_{G,0,F,0}(t) = \{G\}\{F\}.$$

Since the curve exhibits rotational symmetry around the $z$ axis, for analysis we will find it useful to derive from (1) the projection of the curve on the $xy$ (equatorial) plane in two equivalent forms

$$proj_{xy}(Cl) = \sin(2\pi[Ft+\beta])e^{i2\pi[Gt+\gamma]} \quad (2)$$

and

$$proj_{xy}(Cl) = \frac{i}{2}(e^{i2\pi[Gt-Ft+\beta-\gamma]} - e^{i2\pi[Gt+Ft+\beta+\gamma]}). \quad (3)$$

Derivatives of the Clelia curve are useful for finding curvature and torsion as well as for rendering. The $n^{th}$ derivative of a Clelia curve is given in complex form by

$$\frac{d^n Cl_{G,\gamma,F,\beta}(t)}{dt^n} =$$

$$\frac{(2\pi)^n}{2} \begin{bmatrix} -\text{Im}([i(G-F)]^n z_{G-F} + [i(G+F)]^n z_{G+F}) \\ \text{Re}([i(G-F)]^n z_{G-F} - [i(G+F)]^n z_{G+F}) \\ 2\text{Re}[(iF)^n z_F] \end{bmatrix} \quad (4)$$

where $z_{G-F} = e^{i2\pi[(G-F)t+\gamma-\beta]}$, $z_{G+F} = e^{i2\pi[(G+F)t+\gamma+\beta]}$, $z_F = e^{i2\pi[Ft+\beta]}$ and $z \in \mathbf{C}$.

### 2.2. Motion Classification and Symmetries

We first define some terminology that helps describe spherical geometry and avoids explicit reference to a Cartesian coordinate system. Figure 1 illustrates these conventions. The primary reference is the *polar axis* that runs across two opposing points on the sphere. In our case, the polar axis is the $z$ axis. The two points where the polar axis intersects the sphere are called the *poles*. A *parallel* is a plane perpendicular to the polar axis. The *equatorial plane* is the parallel that intersects the center of the sphere. A *meridional plane* is any plane that contains the polar axis.
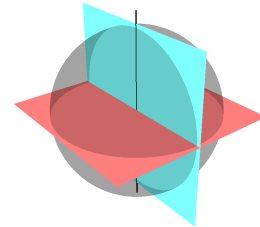


**Figure 1:** A sphere with illustrations of its equatorial plane (red), meridional plane (cyan), and polar axis (black).

In general, a Clelia curve will exhibit a motion that is biased

with respect to some polar axis. There are three basic patterns: meridional, parallel, and mixed (Figure 2). Meridional motions move mostly through the polar axis, that is along spherical meridians or lines of longitude, and have $|G| \ll |F|$. Parallel motions move mostly around the polar axis, that is along spherical parallels or lines of latitude, and result when $|G| \gg |F|$. Mixed motions move equally through and around the poles and result when $|G| \approx |F|$.



**Figure 2:** Basic motions of a Clelia curve. From left to right are meridional ($\{1\}\{20\}$), parallel ($\{20\}\{1\}$), and mixed ($\{10\}\{11\}$) motions.

A Clelia curve exhibits $n$-fold rotational symmetry around the polar axis where $n = F'$. Furthermore, the curve can exhibit one of two types of reflection symmetry about the equatorial plane (Figure 3). For $F', G'$ both odd and non-zero, the curve has prismatic symmetry (standard reflection, $D_{nh}$ in Schoenflies notation), for just one odd it has antiprismatic symmetry (reflection followed by $1/2n$ rotation about the polar axis, $D_{nd}$). As $F', G'$ are coprime, they cannot both be even. Curves with even-fold rotational symmetry, other than the trivial case $\{0\}\{1\}$, cannot exhibit prismatic symmetry. A final symmetry worth noting is that for odd $G'$ and even $F'$, the shape remains invariant under changes of sign of $G'$ and $F'$.
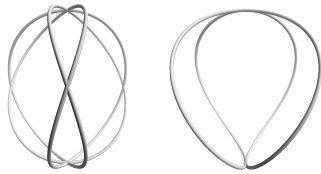


**Figure 3:** Clelia curves belong to one of two symmetry groups: prismatic ($D_{nh}$) or antiprismatic ($D_{nd}$). The left curve $\{1\}\{3\}$ has $D_{3h}$ symmetry and the right curve $\{1\}\{2\}$ has $D_{2d}$ symmetry.

## 3. Sum of Clelia Curves

A single Clelia curve lies on the surface of a sphere. To generate curves that are not constrained to lying on a sphere, we can use a linear combination of $K$ Clelia curves

$$\sum_{k=1}^{K} A_k \{G_k, \gamma_k\} \{F_k, \beta_k\} \qquad (5)$$

where $A_k \in \mathbf{R}$ is the amplitude of the $k^{th}$ Clelia curve and $G_k, F_k$ must be coprime to avoid a multiply-wound curve. For convenience, we call the special case for $K = 2$ a *biclelia* curve. The rest of this section discusses symmetry and other aspects common to all sums of Clelia curves. The remaining sections cover specific interesting subclasses of (5).

### 3.1. Envelope Form

While (5) describes all possible shapes from a sum of Clelia curves, it does not effectively capture the more interesting families of shapes that were uncovered through empirical investigation nor have enough structure to predict the symmetries of the resulting curves. For this reason, we define the *envelope form* as a subset of (5) to be

$$\sum_{k=1}^{K} A_k \{g_k \sigma + c_k \ell, \gamma_k\} \{f_k \sigma + b_k \ell, \beta_k\} \qquad (6)$$

where $\sigma, \ell \in \mathbf{Z}$ are winding frequencies, $f_k, g_k, c_k, b_k \in \mathbf{Z}$ are envelope shaping parameters. The envelope is most visible for $g_k, f_k, c_k, b_k \ll |\sigma| + |\ell|$. This form is convenient as it allows independent control over the shape of the curve's envelope and the winding pattern that sweeps out the envelope. As $|\sigma| + |\ell|$ increases, the density of the curve increases and subsequently the envelope becomes more visible. $b_k$ and $c_k$ are largely responsible for the shape of the envelope intersecting meridional planes while $g_k$ influences its shape on parallel planes.

For subsequent discussion, we define $x_\Delta$ to be the largest modulus so that all pairs in $(x_1, x_2, \ldots, x_K)$ are congruent modulo $x_\Delta$. Parameter sets where $g_\Delta = \ell$, $f_\Delta = \ell$, $c_\Delta = \sigma$, or $b_\Delta = \sigma$ are generally not helpful as they reduce to a simplified set of parameters. For example, if $g_\Delta = \ell$ we can move some integer multiple of $\ell$ from each $g_k \sigma$ into $c_k \ell$ resulting in a new set of $g_k$ that are all equal. Additionally, when $f_k = 0$, the envelope remains invariant along the line $c_k + m g_k$ for $m \in \mathbf{N}$. Moving along the line by $m$ simply results in a change in the winding $\sigma \to \sigma + m\ell$ as $g_k \sigma + (c_k + m g_k)\ell = g_k(\sigma + m\ell) + c_k \ell$.

### 3.2. Symmetry

This section outlines some of the symmetry properties common to all curves. While symmetry is interesting in its own right, another strong motivation for understanding symmetry is that it also allows a better understanding of asymmetry. In effect, by breaking the rules that produce symmetry, we obtain asymmetry.

For a sum of $K$ Clelia curves, the symmetry characteristics of the resulting curve are less straightforward than for a single Clelia curve. For example, the cyclic symmetry of the curve around the polar axis is $\gcd(G_\Delta, F_1, F_2, \ldots, F_K)$. This can be derived from (3) along with the relationship between the frequencies and cyclic symmetry of sums of harmonic complex sinusoids plotted on the complex plane [Far96, Put12]. Table 1 lists the parameter constraints of (6) that produce a curve with one of three types of axial symmetry $C_{nv}$, $D_{nh}$, or $D_{nd}$. Figure 4 shows a classification of the axial symmetries under consideration. $C_{nv}$ has an $n$-fold rotation axis with $n$ reflection planes through the axis of symmetry while $D_{nh}$ (prismatic) and $D_{nd}$ (antiprismatic) have $C_{nv}$ symmetry with the addition of a reflection or roto-reflection plane, respectively, perpendicular to the axis of rotation. All curves have constraints $g_k = 1, f_k = 0$ to maintain $\ell$-fold rotational symmetry. In general, for non-zero values of phases $\gamma_k, \beta_k$, the $C_{nv}$, $D_{nh}$ and $D_{nd}$ symmetries break into $C_n$, $C_{nh}$ and $S_{2n}$ symmetries, respectively, as the reflection planes intersecting the axis of rotation vanish. Like the individual Clelia curves, we did not find any curves with $D_{nh}$ for even $n$.

| Curve Symmetry | $\ell$ | $\sigma$ | $c_k$ | $b_k$ |
|---|---|---|---|---|
| $C_{\ell v}$ | any | any | any | any |
| $D_{\ell h}$ | odd | odd | even | odd |
| | odd | even | odd | |
| $D_{\ell d}$ | odd | even | even | |
| | odd | odd | odd | |
| | even | odd | even | |
| | even | odd | odd | |

**Table 1:** Symmetry characteristics of curves produced from a linear combination of Clelia curves given by (6) with $g_k = 1, f_k = 0$ and $\gamma_k = \beta_k = 0$.

| Envelope Symmetry | $g_k$ | $c_k$ | $f_k$ | $b_k$ |
|---|---|---|---|---|
| $C_{\infty v}$ | 1 | any | 0 | any |
| $C_{nv}$ | $g_\Delta = n$ | any | $mn$ | any |
| $D_{\infty h}$ | 1 | even, odd | 0 | odd |
| $D_{nh}$ | $g_\Delta = n$ | odd | $mn$ | odd |
| $D_{nh}$ | $g_\Delta = n$ even | even | $mn$ | odd |
| $D_{nd}$ | $g_\Delta = n$ odd | even | $mn$ | odd |

**Table 2:** Parameter constraints for envelope symmetries of curves produced from a linear combination of Clelia curves with $\gamma_k = \beta_k = 0$. 'Odd' and 'even' designate all values of that type are odd or even, respectively. 'Any' specifies that the values are not all odd or even.

The following sections present basic families of shapes that may be used as a starting point for creating of more complex curves.

## 4. Surface of Revolution

Perhaps the simplest family of shapes from (6) generates a curve whose envelope is a surface of revolution (SOR). A SOR is the surface swept out by revolving a two-dimensional curve, the generatrix, around an axis of revolution [KI15]. A SOR exhibits $C_\infty$ symmetry with respect to its axis of revolution. The curve is given by

$$\sum_{k=1}^{K} A_k \{\sigma\}\{b_k \ell, \beta_k\} \tag{7}$$

where $\sum_{k=1}^{K} A_k\{0\}\{b_k, \beta_k\}$ is the generatrix—a sum of complex sinusoids. We call this curve a *K-circloid SOR* where a *K*-circloid is a sum of *K* harmonic complex sinusoids. If $b_k$ are odd, then the envelope exhibits reflection symmetry about the equatorial plane, in agreement with Table 2. We next consider a selection of SORs with a small number of components as they relate to several well-known basic shapes that are useful starting points for creating more complex shapes.

The *bicircloid SOR* is the simplest case of (7) having a 2-circloid (also called a bicircloid [Nor68] or centered trochoid) as a generatrix. Bicircloids form a superset of such curves as ellipses, rose curves, and centered cycloids. A bicircloid SOR is given by

$$A_1\{\sigma\}\{b_1 \ell\} + A_2\{\sigma\}\{b_2 \ell, \beta_2\} \tag{8}$$

where $\beta_2$ controls the rotation angle on the meridional plane of the bicircloid generatrix $A_1\{0\}\{b_1\} + A_2\{0\}\{b_2, \beta_2\}$. When $\sigma = 0, \ell = 1$, we obtain the generatrix itself. Parameters for some basic SORs are summarized in Table 3. A torus (knot) is produced from an eccentric circle generatrix and a spheroid from a ellipse generatrix. Basic shapes including a cone, bicone, and cylinder can be generated by using a generatrix that is the two lowest frequency components of the Fourier series of a regular polygon [Rob94]. For a regular *n*-gon, one may use $b_1 = -1, b_2 = n - 1, A_1 = (n-1)^2 A_2$.

The basic bicircloid SOR shapes can be used as a starting point
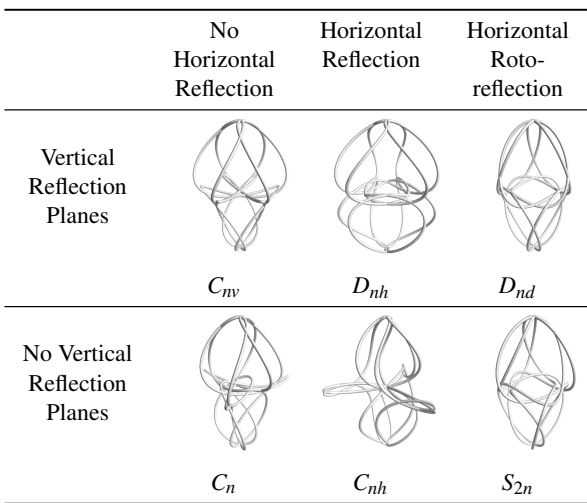


**Figure 4:** Examples of axial symmetry groups. All figures have *n*-fold rotational symmetry around a central vertical axis. The groups are distinguished by lack or presence of specific reflection planes. The columns distinguish the nature of reflection symmetry about a central horizontal plane. The figures on the top row have reflection symmetry about *n* vertical planes through the axis of rotational symmetry while those on the bottom row do not.

The cyclic symmetry of the envelope has a minimum value $g_\Delta$ where $g_\Delta$ is defined as above. The envelope exhibits reflection symmetry when all $b_k$ are odd and $c_\Delta$ is even (all $c_k$ are even or all $c_k$ are odd). Other envelope symmetries are given in Table 2. In general, these symmetries are valid only when $c_k$ or $b_k$ have at least two differing values. Conspicuously absent from the table is the symmetry group $D_{nd}$ for even *n*. This group is possible to create, however, the rules are more complex than the other cases. There must be at least one component from the following two families: 1) $g_k = 1 \pm 2mn$ and 2) $g_k = 1 \pm (2m+1)n$. The parity of $c_k$ must differ between the two families (i.e., if family 1 has odd $c_k$, then family 2 must have even $c_k$ and vice versa). $f_k$ may be $2mn$. Note that each family has $D_{2nh}$ symmetry.

| Curve Envelope | $b_1$ | $b_2$ | $A_k$ | $\beta_2$ |
|---|---|---|---|---|
| Torus | 1 | 0 | $A_1 < A_2$ | $\frac{1}{4}$ |
| Oblate spheroid | $-1$ | 1 | $-A_1 < A_2 < 0$ | 0 |
| Prolate spheroid | $-1$ | 1 | $0 < A_2 < A_1$ | 0 |
| Double cone | $-1$ | 1 | $A_1 = A_2$ | $\frac{1}{4}$ |
| Cone | $-1$ | 2 | $A_1 = 4A_2$ | 0 |
| Bicone | $-1$ | 3 | $A_1 = 9A_2$ | 0 |
| Closed Cylinder | $-1$ | 3 | $A_1 = -9A_2$ | 0 |
| Apple | 1 | 2 | $A_1 = -2A_2$ | 0 |

**Table 3:** Parameters used in (8) to generate curves with envelopes in the shape of basic surfaces of revolution.

for producing more complex shapes. For instance, adding one more component to a spheroid SOR allows generation of a variety of rod- and disc-like shapes (Figure 5).



**(a)**     **(b)**     **(c)**
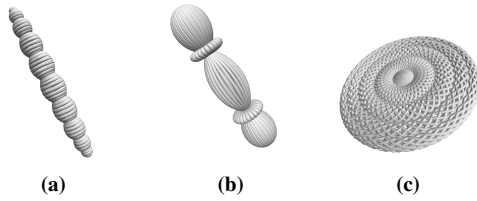
**Figure 5:** Rod- and disc-like shapes generated by adding one extra component to a spheroid SOR:
**(a)** $\{\sigma\}\{\ell\} + \frac{4}{5}\{\sigma\}\{-\ell\} + \frac{5}{100}\{\sigma\}\{20\ell\}$ with $\sigma = 180, \ell = 1$,
**(b)** $\{\sigma\}\{\ell\} + \{\sigma\}\{-\ell\} + \frac{1}{2}\{\sigma\}\{5\ell\}$ with $\sigma = 1, \ell = 26$ and
**(c)** $\{\sigma\}\{\ell\} - \frac{4}{5}\{\sigma\}\{-\ell\} + \frac{5}{100}\{\sigma\}\{20\ell\}$ with $\sigma = 41, \ell = 40$.

Toroidal shapes are produced by moving the center of the generatrix off the axis of revolution through an additional Clelia component. The offset combined with (7) results in

$$B\{\sigma\}\{0, 1/4\} + \sum_{k=1}^{K} A_k\{\sigma\}\{b_k\ell, \beta_k\} \qquad (9)$$

where $B$ controls the distance from the center of the $K$-circloid to the axis of revolution. If the generatrix is an eccentric ellipse, an elliptic torus [KI15] results. If the generatrix is an eccentric Tusi couple, the SOR forms an open cylinder or open conical frustum. Table 4 summarizes the parameters that may be used to generate these envelope shapes.

A more general class of SOR, that we call a *K-Clelia SOR*, has a sum of Clelia curves as a generatrix. It is a special case of (6) given by

$$\sum_{k=1}^{K} A_k\{\sigma + c_k\ell\}\{b_k\ell, \beta_k\} \qquad (10)$$

where $\sum_{k=1}^{K} A_k\{c_k\}\{b_k, \beta_k\}$ is the generatrix. The envelope is invariant under the mapping $c_k \to c_k + \delta$ as this implies $\sigma \to$

| Curve Envelope | $b_1$ | $b_2$ | Amplitudes | $\beta_k$ |
|---|---|---|---|---|
| Elliptic Torus | $-1$ | 1 | $A_1 \neq A_2$ | 0 |
| Open Cylinder | $-1$ | 1 | $A_1 = A_2$ | 0 |
| Conical Frustum | $-1$ | 1 | $A_1 = A_2 = \frac{\sqrt{2}}{2}B$ | $\beta_1 = \beta_2$, $\beta_k \in (0, \frac{1}{8})$ |

**Table 4:** Parameters used in (9) to generate a special class of curves with envelopes in the shape of an elliptic torus.

$\sigma + \delta\ell$. Thus, $\sum c_k$ should be small to achieve the most accurate winding pattern in terms of $\sigma, \ell$. When all $c_k$ are equal, the curve degenerates into a $K$-circloid SOR. For $K = 2$, we get a *biclelia SOR* given by

$$A_1\{\sigma + c_1\ell\}\{b_1\ell\} + A_2\{\sigma + c_2\ell\}\{b_2\ell, \beta_2\}. \qquad (11)$$

Table 5 lists various shape motifs along with examples of some of these curves.

## 5. Meridional Sweep Surface

A *meridional sweep surface* has an envelope that is the spherical product of a $K$-circloid on the equatorial plane and a circle or ellipse on the meridional plane. A curve whose envelope has this shape is given by

$$\sum_{k=1}^{K} A_k\{g_k\sigma\}\{\ell\}. \qquad (12)$$

From (2), the curve's envelope on the equatorial plane is found to be $\pm\sum_{k=1}^{K} A_k e^{i2\pi g_k t}$. The envelope always has even-fold rotational symmetry; $g_\Delta$ if $g_\Delta$ is even and $2g_\Delta$ if $g_\Delta$ is odd. The shape is oblate when $\text{sgn}(A_k)$ includes both $-1$ and $1$ and flattens completely as $\sum_{k=1}^{K} A_k \to 0$. The flattening is due to destructive interference of the sinusoids along the polar axis of the individual Clelia curves. Figure 6 shows several examples of these curves having $K = 2$ or $K = 3$ components.
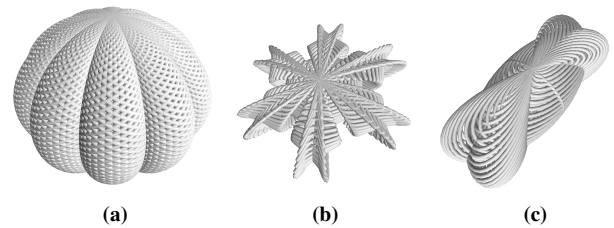


**(a)**     **(b)**     **(c)**

**Figure 6:** Examples of meridional sweep surfaces:
**(a)** $\{\sigma\}\{\ell\} - \frac{1}{10}\{11\sigma\}\{\ell\}$ with $\sigma = 80, \ell = 81$,
**(b)** $\frac{1}{2}\{-5\sigma\}\{\ell\} - \{\sigma\}\{\ell\} + \frac{1}{5}\{10\sigma\}\{\ell\}$ with $\sigma = 51, \ell = 50$ and
**(c)** $\{2\sigma\}\{\ell\} + \{\sigma\}\{\ell\} - \{-\sigma\}\{\ell\}$ with $\sigma = 51, \ell = 50$.
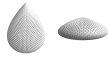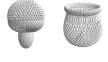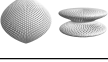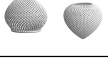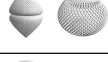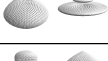
| Shape Motifs | | | $\lvert c_2 - c_1 \rvert$ | $b_1$ | $b_2$ |
|---|---|---|---|---|---|
| Teardrop, egg, water bead | | | 1 | ±1 | 1 |
| Gumdrop, punted cone | | | 1 | ±1 | 2 |
| Mushroom, pot | | | 1 | ±1 | 3 |
| Urn, mushroom | | | 1 | ±1 | 4 |
| Conical sphere, spool | | | 2 | −1 | 1 |
| Onion dome, top | | | 2 | −1 | 2 |
| Bicone, cratered sphere | | | 2 | −1 | 3 |
| Peanut, capsule, lentoid | | | 2 | 1 | 1 |
| Bell, vase | | | 2 | 1 | 2 |
| Torus-dumbell, hourglass | | | 2 | 1 | 3 |
| Perfume bottle, pear, lid | | | 3 | ±1 | 1 |
| Knob, pear, onion dome | | | 3 | ±1 | 2 |
| Acorn, pot | | | 3 | ±1 | 3 |

**Table 5:** Shape motifs for parameters of a biclelia surface of revolution given by (11). The motifs within each row morph continuously into one another through changes in $A_k$.

## 6. Modulated Surface of Revolution

We can generalize (7) and (12) into a single family of curves with envelopes resembling a SOR but with a finite order of rotational symmetry. This *modulated surface of revolution* is given by

$$\sum_{k=1}^{K} A_k \{g_k \sigma\}\{b_k \ell\} \tag{13}$$

where $g_k, b_k$ influence the shape of the envelope on parallel and meridional planes, respectively. Like the meridional sweep surface, the envelope always has even-fold rotational symmetry.

A special case of (13) produces a *distorted Clelia*. The distortion leaves the self-intersection points of the Clelia curve intact, thus, the distorted curve is homeomorphic to the original Clelia curve (Figure 7). It is given by

$$\{\sigma\}\{\ell\} + \sum_{k=2}^{K} A_k \{g_k \sigma\}\{b_k \ell\} \tag{14}$$

where $g_k$ are odd, $A_k$ determine the amount of distortion and $\sum_{k=2}^{K} \lvert A_k \rvert < 1$. Since $g_k$ must be odd, the rotational symmetry of the envelope is limited to even orders. When all $b_k$ are odd, the envelope exhibits reflection symmetry about the equatorial plane. Each component given by $k$ introduces a particular shaping effect. $b_k$ correlates to the number of distortion 'planes' along parallels. When $g_k > 0$, the distortion is largely convex and when $g_k < 0$ it is largely concave. We will next examine some special cases of the distorted Clelia.
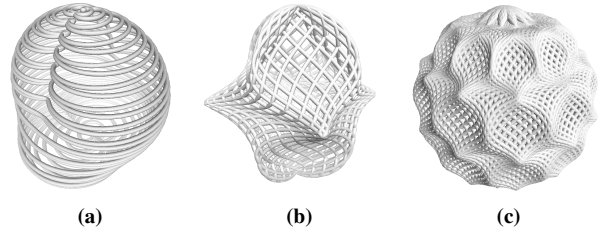


**Figure 7:** Examples of distorted Clelia curves:
**(a)** $\{\sigma\}\{\ell\} + \frac{1}{4}\{3\sigma\}\{2\ell\}$ with $\sigma = 41, \ell = 1$,
**(b)** $\{\sigma\}\{\ell\} + \frac{1}{4}\{-3\sigma\}\{3\ell\}$ with $\sigma = 31, \ell = 30$ and
**(c)** $\{\sigma\}\{\ell\} + \frac{1}{20}\{-11\sigma\}\{11\ell\}$ with $\sigma = 101, \ell = 100$.

For some curves, the envelope on slices through meridional planes reveal bicircloid curves (Figure 8). A 'trip-let' [Hof79] is a three-dimensional geometric object whose projections on orthogonal planes reveal distinct shapes with no obvious correlation. The slice shapes are given by the bicircloids $A_1\{b_1\} + A_2\{\pm b_2\}$.



**Figure 8:** The distorted Clelia curve $\{\sigma\}\{\ell\} + \frac{1}{2}\{-\sigma\}\{2\ell\}$ (left) along with slices through perpendicular meridional planes (middle and right). The meridional plane slices reveal a cardioid and deltoid.

A special case of (14) produces a variety of polyhedral-like shapes such as prisms (distorted cylinder), pyramids and platonic solids including the octahedron and cube. The general equation is

$$\{\sigma\}\{\ell\} + A_2\{\sigma\}\{b_2\ell\} + A_3\{g_3\sigma\}\{\ell\} \tag{15}$$

where $g_3$ dictates the rotational symmetry of the envelope and $b_2$ determines the shape of the curve on the meridional plane. When $b_2, g_3 < 0$, the geometry of the envelope is largely concave and permits formation of flatter faces. Table 6 presents parameter constraints of some polyhedral motifs and Figure 9 shows some particular instances.

| Envelope Motif | Constraints | | |
|---|---|---|---|
| | $b_2$ | $g_3$ | $A_k$ |
| Elliptical Cone | $-2$ | $-1$ | - |
| Pyramid | $-2$ | $< 0$ | - |
| Bipyramid | $-3$ | $< 0$ | $A_2 > 0$ |
| Prism | $-3$ | $< 0$ | $A_2 < 0$ |
| Cube | $-3$ | $-3$ | $A_2 < 0, A_2 = A_3$ |
| Elongated Pyramid | $-4$ | $< 0$ | - |
| Elongated Bipyramid | $-5$ | $< 0$ | $A_2 > 0$ |
| Bifrustum | $-5$ | $< 0$ | $A_2 < 0$ |

**Table 6:** Parameter constraints for generating specific polyhedral envelope shapes from (15).



**(a)**      **(b)**      **(c)**
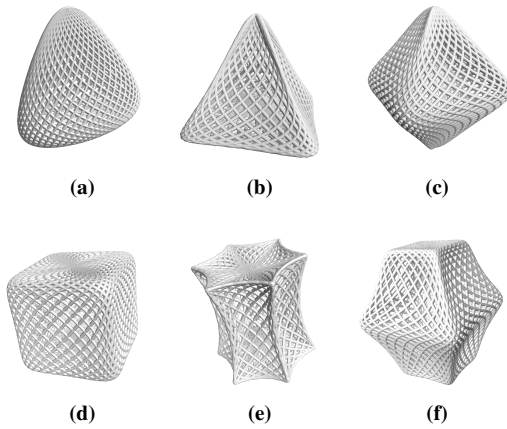
**(d)**      **(e)**      **(f)**

**Figure 9:** Examples of distorted Clelia curves having polyhedral envelope shapes:
**(a)** elliptical cone $\{\sigma\}\{\ell\} + \frac{1}{4}\{\sigma\}\{-2\ell\} + \frac{1}{2}\{-\sigma\}\{\ell\}$,
**(b)** square pyramid $\{\sigma\}\{\ell\} + \frac{1}{3}\{\sigma\}\{-2\ell\} - \frac{1}{5}\{-3\sigma\}\{\ell\}$,
**(c)** square bipyramid $\{\sigma\}\{\ell\} + \frac{3}{20}\{\sigma\}\{-3\ell\} + \frac{3}{20}\{-3\sigma\}\{\ell\}$,
**(d)** cube $\{\sigma\}\{\ell\} - \frac{15}{100}\{\sigma\}\{-3\ell\} - \frac{15}{100}\{-3\sigma\}\{\ell\}$,
**(e)** hexagonal prism $\{\sigma\}\{\ell\} - \frac{1}{3}\{\sigma\}\{-3\ell\} + \frac{1}{5}\{-5\sigma\}\{\ell\}$ and
**(f)** square bifrustum $\{\sigma\}\{\ell\} - \frac{1}{10}\{\sigma\}\{-5\ell\} + \frac{1}{5}\{-3\sigma\}\{\ell\}$
where $\sigma = 40, \ell = 41$ for all figures.

## 7. Bicircloid Screw Surface

A *bicircloid screw surface* is similar to a meridional sweep surface, however, its generatrix may also twist as it oscillates along the polar axis resulting in an overall screw-like motion. The twisting allows the envelope to have both even and odd orders of rotational symmetry unlike the related surfaces described above. A curve having this envelope shape is given by

$$A_1\{g_1\sigma + c_1\ell\}\{\ell\} + A_2\{g_2\sigma + c_2\ell\}\{\ell\}$$

where the generatrix is the bicircloid $A_1 e^{i2\pi g_1 t} + A_2 e^{i2\pi g_2 t}$. The curve is composed of $\sigma$ repetitions of the generatrix that

simultaneously makes $\ell$ oscillations along the polar axis while twisting a total of $\frac{360(c_1 g_2 - c_2 g_1)\ell}{g_2 - g_1}$ degrees around the polar axis. The envelope has an overall Clelia 'motif' corresponding to $\{g_2 c_1 - g_1 c_2\}\{g_2 - g_1\}$ and rotational symmetry $|g_1 - g_2|$. If the generatrix happens to be a hypocycloid, its cusps clearly trace out a Clelia curve (Figure 10a). When the Clelia is degenerate, then multiple equiangular copies of the Clelia will typically occur in the completed pattern. When $c_1 = c_2 = 0$, there is no twisting action and the curve falls back to a meridional sweep surface. When $g_1 = g_2$ the generatrix becomes a circle which results in a biclelia SOR curve. When $\text{sgn}(A_1) \neq \text{sgn}(A_2)$, the curve is circumscribed by an oblate spheroid with a height along the polar axis of $2|A_1 + A_2|$ and a radius of $|A_1 - A_2|$ (Figures 10b and 10c).
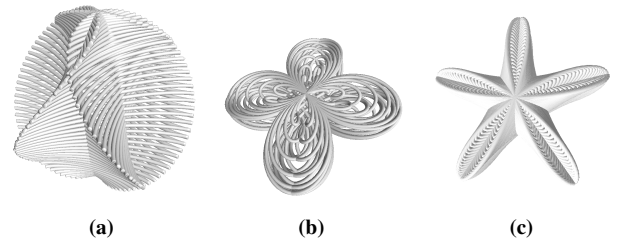


**(a)**      **(b)**      **(c)**

**Figure 10:** Examples of bicircloid screw surfaces:
**(a)** $\{-\sigma\}\{\ell\} + \frac{1}{2}\{2\sigma + 2\ell\}\{\ell\}$ with $\sigma = 101, \ell = 1$,
**(b)** $\{-\sigma + \ell\}\{\ell\} - \frac{7}{10}\{3\sigma - \ell\}\{\ell\}$ with $\sigma = 35, \ell = 37$ and
**(c)** $\{2\sigma + \ell\}\{\ell\} - \frac{2}{3}\{-3\sigma - \ell\}\{\ell\}$ with $\sigma = 61, \ell = 100$.

## 8. Ruled Surface Clelia

A *ruled surface Clelia* is a curve that lies on a ruled surface whose line generatrix endpoints sweep out a Clelia curve. We present two unique ways of generating a ruled surface Clelia.

The first type of ruled surface Clelia we denote an *axial ruled surface Clelia* as its development is biased with respect to the polar axis (Figure 11). A curve having this envelope shape is given by

$$\{-\sigma + c\ell\}\{b\ell\} + \{\sigma + c\ell\}\{b\ell\}$$

where the outer edge of the curve envelope is described by the Clelia curves $\{\pm c\}\{b\}$. When $c$ is odd and $b$ is even, these Clelia curves overlap and for other parity of $c$ and $b$, the envelope is reflected about the meridional plane. The curve is closely related to a bicircloid screw surface having a Tusi couple as the generatrix. It should be noted that a generalized version using $c_1$ and $c_2$ in place of the respective $c$ is also valid, however, the envelope edge has a more complex description as $\{\pm(c_1 + c_2)\}\{2b\}$. The winding frequencies are slightly unusual in that $\sigma$ determines the amount of oscillation parallel to the equatorial plane and through the polar axis while $\ell$ determines the amount of motion through the poles. The curve intersects the poles of its spherical envelope $b\ell$ times. When $c = 0, b = 1$, we obtain a flat disc that is the projection of the Clelia curve $\{\sigma\}\{\ell\}$ on the meridional plane.

From (2), we find that the equatorial projection of the curve is $2\cos(2\pi\sigma t)\cos(2\pi b\ell t)e^{i2\pi c\ell t}$. The projection can be interpreted as a cosine amplitude modulation of the rose

curve $2\cos(2\pi b\ell t)e^{i2\pi c\ell t}$. The envelope of the projection is $\pm 2\cos(2\pi bt)e^{i2\pi ct}$. When $\sigma \ll \ell$, the modulation is slow and the rose curve is fast. The curve develops as $\sigma$ continuous morphs of $\ell$ cycles of the rose curve $2\cos(2\pi bt)e^{i2\pi ct}$. Conversely, when $\sigma \gg \ell$, the modulation is fast and the rose curve is slow. Here, the curve develops as $\sigma$ rapid oscillations between the rose curves $\pm 2\cos(2\pi bt)e^{i2\pi ct}$. In general, we get $\sigma$ oscillations between $\ell$ cycles of the rose curves $\pm 2\cos(2\pi bt)e^{i2\pi ct}$.
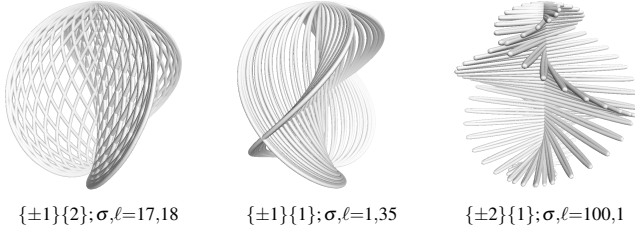


**Figure 11:** Examples of axial ruled surface Clelia curves. The equation of the envelope $\{c\}\{b\}$ is given under each curve along followed by the the winding frequencies $\sigma, \ell$.

The second type of ruled surface Clelia we call an *isotropic ruled surface Clelia* as the surface is swept out from an amplitude modulation (Figure 12). A curve having this envelope shape is given by

$$\{g\sigma\}\{\lceil f\sigma \rceil - \ell\} + \{g\sigma\}\{\lfloor f\sigma \rfloor + \ell\} \qquad (16)$$

where the envelope is $\pm\{g\}\{f\}$. From (1) and some basic trigonometry, one finds that (16) is equivalent to $2\cos(2\pi\ell t)\{g\sigma\}\{f\sigma\}$. The curve development can be interpreted as $\sigma$ cycles of the Clelia curve $\{g\}\{f\}$ undergoing a cosine amplitude modulation. When $\sigma \gg \ell$, the curve develops as a slow modulation between $\pm\{g\}\{f\}$. When $\sigma \ll \ell$, the curve oscillates rapidly between $\pm\{g\}\{f\}$.
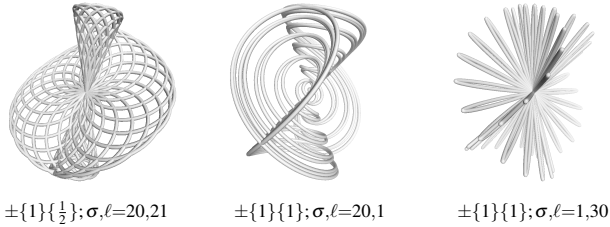


**Figure 12:** Examples of isotropic ruled surface Clelia curves. The equation of the envelope $\pm\{g\}\{f\}$ is given under each curve along followed by the the winding frequencies $\sigma, \ell$.

## 9. Twisted Torus

A *twisted torus* (or twisted surface [GAS06]) is like a torus, but with two key differences in its generatrix: it is non-circular and it slowly rotates on its local coordinate plane as it revolves around the axis of revolution. A curve lying on a twisted torus is given by

$$A_{min_1}\{\sigma\}\{b_1(\ell+\Delta)\} + A_{min_2}\{\sigma\}\{f\sigma + b_2(\ell+\Delta)\}$$
$$+ A_{maj}\{\sigma\}\{0, \tfrac{1}{4}\} \qquad (17)$$

where $A_{maj}$ is the major radius of the torus, $A_{min_1}\{0\}\{b_1\} + A_{min_2}\{0\}\{b_2\}$ is the generatrix, $|b_2| > |b_1|$, $f/(b_2 - b_1)$ is the number of twists of the generatrix over one revolution.

An optional parameter $\Delta \in \mathbf{Z}$ is used to correct the winding pattern to that expected from $\sigma, \ell$. The winding correction is generally most helpful when $\sigma \gg \ell$. We use

$$\Delta = \text{nint}(f\sigma/(b_1 - b_2)) \qquad (18)$$

where nint is the nearest integer function. The condition $b_1\Delta - (f\sigma + b_2\Delta) \cong 0$ stipulates an even spread of the twisting term, $f\sigma$, across the two components containing $\Delta$. Figure 13 shows the twisted torus curve $3\{\sigma\}\{-(\ell+\Delta)\} + \{\sigma\}\{f\sigma + 3(\ell+\Delta)\} + 8\{\sigma\}\{0, \tfrac{1}{4}\}$ with $\sigma = 25, \ell = 1$. On the left is the curve with no twist ($f = 0$) showing the expected winding pattern. In the middle is the same shape with twist $f = 8$ applied. Here, it is evident that the original winding pattern is distorted. The right figure is the same as the middle, but with winding correction $\Delta = -50$ applied. It more closely matches the expected winding pattern when there is no twist.
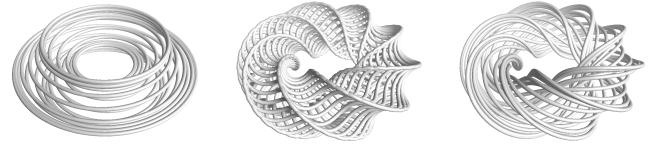


**Figure 13:** Winding correction for twisted torus curves $3\{\sigma\}\{-(\ell+\Delta)\} + \{\sigma\}\{f\sigma + 3(\ell+\Delta)\} + 8\{\sigma\}\{0, \tfrac{1}{4}\}$ with $\sigma = 25, \ell = 1$. These show the curve with (left to right) no twist ($f = 0$), twist $f = 8$, and twist $f = 8$ with winding correction from (18).

When the generatrix in (17) is a Tusi couple the curve lies on a *twisted circular ribbon* given by

$$\frac{A_{min}}{2}(\{\sigma\}\{\ell\} + \{\sigma\}\{f\sigma - \ell\}) + A_{maj}\{\sigma\}\{0, \tfrac{1}{4}\}. \qquad (19)$$

The envelope forms an orientable or non-orientable surface for $f$ odd or even, respectively. When $f = 1$, the curve lies on a Moebius strip. When $A_{maj} = 0$, the curve degenerates into an isotropic ruled surface Clelia.
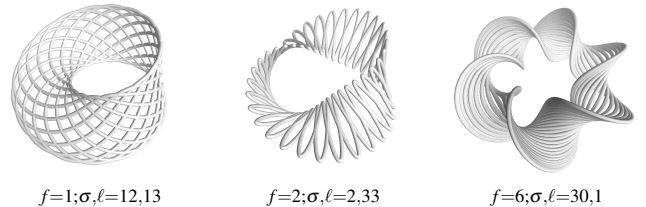


**Figure 14:** Examples of twisted circular ribbon curves produced from (19) with $A_{min} = \frac{1}{2}$ and $A_{maj} = 1$. The leftmost curve lies on a Moebius strip. The rightmost figure has the winding correction from (18) applied.

## 10. Canal Curve

A *canal curve* is a curve whose path sweeps out the interior of a canal surface—the envelope formed by a sphere moving along a directrix curve [Mon50]. The curve is given by

$$A_1\{c_1\}\{b_1\} + \sum_{k=2}^{K} A_k\{c_k\ell\}\{b_k\ell\} \qquad (20)$$

where $A_1\{c_1\}\{b_1\}$ is the spherical generatrix, $\sum_{k=2}^{K} A_k\{c_k\}\{b_k\}$ is the directrix of the canal, $A_1$ is the radius of the canal and $\ell$ is the number of orbits the generatrix makes along the directrix. Here, the generatrix simultaneously unfolds as it translates along the directrix. For adequate visibility of the directrix path, a general rule of thumb is $A_1 < \frac{1}{4}\sum_{k=2}^{K}|A_k|$. Larger values of $A_1$ may begin to mask the directrix depending on the overall complexity of the directrix curve. Figure 15 presents several examples of canal curves. In Figure 15a, the directrix is a circle on a meridional plane, therefore the canal envelope is a torus. In Figure 15b, since $\ell \gg c_1$ and $\ell \gg b_1$, the motion is dominated by orbits along the directrix leading to a more fibrous presentation not unlike a chaotic attractor. Finally, Figure 15c illustrates the possibility of more patterned windings.
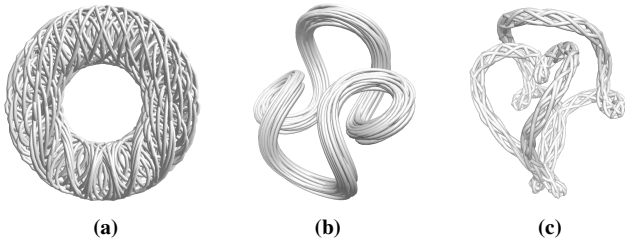


**Figure 15:** Examples of canal curves given by (20):
**(a)** $\frac{2}{5}\{10\}\{170\} + \{0\}\{\ell\}$ with $\ell = 21$,
**(b)** $\frac{1}{5}\{3\}\{1\} + \{0\}\{\ell\} + \{2\ell\}\{3\ell\}$ with $\ell = 31$ and
**(c)** $\frac{1}{10}\{1\}\{168\} + \{\ell\}\{2\ell\} + \frac{1}{2}\{3\ell\}\{5\ell\}$ with $\ell = 9$.

A special case of a canal curve produces a sequence of tubular *fiber bundles* developing along some directrix. It is given by

$$A_1\{\sigma\}\{b_1\ell\} + \sum_{k=2}^{K} A_k\{c_k\ell\}\{b_k\ell\} \qquad (21)$$

where $A_1$ is the maximum radius of the bundles and $A_1\{0\}\{b_1\} + \sum_{k=2}^{K} A_k\{c_k\}\{b_k\}$ is the directrix. The fibers have a fusiform shape forming bundles that are tapered at both ends and generally follow a spiral-like path (Figure 16). The curve consists of $2b_1$ fiber bundles each having $\ell$ fibers. The rotational symmetry of the envelope is $\gcd(b_1, b_2, \ldots, b_k, c_\Delta)$. When $\sigma \ll \ell$, the fibers run mostly parallel forming sheaves (Figure 16a). Conversely, when $\sigma \gg \ell$, the fibers form coils with loops that are nearly parallel to the equatorial plane (Figure 16b). Figure 16c presents a more complex fiber bundle having many bundles and a relatively large bundle radius to mask the directrix curve.
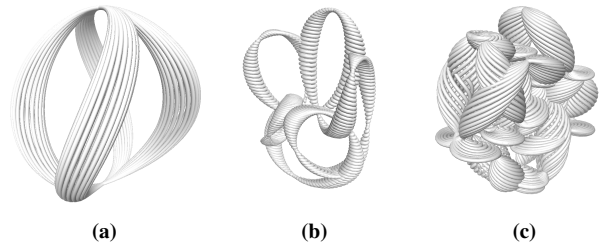


**Figure 16:** Examples of fiber bundle curves produced from (21):
**(a)** $\frac{1}{5}\{\sigma\}\{2\ell\} + \{\ell\}\{2\ell\}$ with $\sigma = 1, \ell = 20$,
**(b)** $\frac{1}{5}\{\sigma\}\{6\ell\} + \{0\}\{-\ell\} + \{\ell\}\{5\ell\}$ with $\sigma = 403, \ell = 1$ and
**(c)** $\frac{2}{5}\{\sigma\}\{26\ell\} + \{6\ell\}\{9\ell\} + \{5\ell\}\{2\ell\}$ with $\sigma = 671, \ell = 13$.

## 11. Weaving

We may add a weaving effect to any modulated surface of revolution described by (13). Two types of plain weaves following an alternating over-under pattern everywhere but at the poles are produced by adding the additional component

$$A_w\{\sigma\}\{\sigma_w\ell, \tfrac{1}{4}\} \qquad (22)$$

where $\sigma_w = 1 \pm 1 \pm \sigma$ or $1 \pm \sigma$ for $\ell$ even or odd, respectively, or

$$A_w\{\sigma + \sigma_w\ell\}\{0, \tfrac{1}{4}\} \qquad (23)$$

where $\sigma_w = \pm\sigma$ or $\pm 1 \pm \sigma$ for $\ell$ even or odd, respectively, and where $A_w$ is the weaving amplitude. For (22), the weave displacement is primarily along meridians while for (23) it is primarily along parallels (Figure 17). The meridional weave has a greater separation of the threads near the poles leading to a more realistic looking weave than the parallel weave. If the curve is rendered as a tube, then a good choice of $A_w$ is the radius of the tube. As $A_w$ increases, the difference in displacement bias between the weaving patterns becomes more apparent.
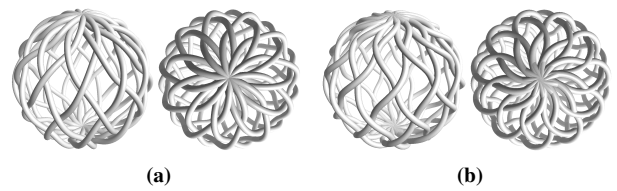


**Figure 17:** Clelia curve $\{7\}\{11\}$ with weaving components added: (a) displacement along meridians with weaving component $\frac{1}{25}\{7\}\{88, \frac{1}{4}\}$ and (b) displacement along parallels with weaving component $\frac{1}{25}\{7 + 88\}\{0, \frac{1}{4}\}$.

## 12. Rendering and Visualization

The output of (5) and (6) is a sequence of points that may be rendered directly as point sprites or line segments between successive points. For 3D curves, these simple rendering approaches typically result in a graphic that is difficult to read due

to lack of surfaces and lighting. This section discusses techniques that may be used to enhance the depth of the curve and add further visual richness.

### 12.1. Geometry

A common approach to rendering curve point sequences is to generate a canal surface [Mon50] by expanding the curve along its normal directions into a tube. Generating a tube requires finding a tangent, normal, and binormal (TNB) frame of orthonormal vectors at each curve point. A TNB frame can be derived from the Frenet-Serret formulas [Fre52, Ser51]. For the curve $r(t)$, we have the full Frenet-Serret apparatus

$$
\begin{aligned}
T &= \dot{r}/|\dot{r}| \\
B &= (\dot{r} \times \ddot{r})/|\dot{r} \times \ddot{r}| \\
N &= B \times T \\
\kappa &= |\dot{r} \times \ddot{r}|/|\dot{r}|^3 \\
\tau &= ((\dot{r} \times \ddot{r}) \cdot \dddot{r})/|\dot{r} \times \ddot{r}|^2
\end{aligned}
\tag{24}
$$

where $\kappa$ is the curvature, $\tau$ is the torsion and $\dot{r}$, $\ddot{r}$, and $\dddot{r}$ are the first, second and third derivatives, respectively, of $r(t)$ with respect to $t$. A well-defined Frenet-Serret TNB frame requires $\dot{r}$ and $\ddot{r}$ to be non-zero. Parallel transport may be used to work around these pitfalls [Bis75, HM95] though it is a recursive algorithm making GPU implementation far from trivial. With (24), a tubed curve may generated *entirely* on the GPU with arbitrary level-of-detail in a single pass. The trick in doing so is to render the tube as a ribbon that spirals around the curve. We draw a triangle strip with $2NM$ vertices where $N$ and $M$ are the tube's length-wise and radial resolutions, respectively. For the $n^{th}$ vertex, we compute the normalized position $t \in [0, 1]$ along the curve $r(t)$ as

$$
t = \frac{\lfloor n/2 \rfloor + M(n \bmod 1)}{NM}
$$

and then the tube vertex position from

$$
V(t) = r(t) + \rho(\cos(2\pi Nt)\mathbf{N} - \sin(2\pi Nt)\mathbf{B})
$$

where $\rho$ is the radius of the tube. One may dynamically modify $N$ and/or $M$ to change the level of detail based on the distance of the curve to the camera. Generally, one may be more liberal with changes to $M$ as this will have less impact on the shape of the curve. Due to the sampling theorem, $N$ should be at least twice the value of the highest frequency value across all Clelia components. However, due to the spiral rendering and twisting artifacts inherent in (24), we found a value of $N$ around ten times the highest frequency to be necessary. This should only be taken as a rule of thumb as even with low-frequency components the rate of variation of $\tau$ may be much higher than $r$.

### 12.2. Curve Property Modulation

We can add more interest to the curves by modulating various properties along its length such as thickness, color or other material attributes. For example, numerous historic light synthesizers use spinning color wheels including Rimington's Colour-Organ [Rim12, pp.63-64], Wilfred's Clavilux [OTB*17] and Laposky's

*Oscillon* synthesizer [Lap69]. A two property modulation function is given by

$$
M(t) = P_1 + I(t)(P_2 - P_1)
$$

where $t \in [0, 1]$ is the position along the curve and $I(t)$ is a periodic interpolation function with frequency $f_m$ and output ranging in $[0, 1]$. If the curve is generated from (6), choosing $f_m$ to be an integer multiple of $\ell$ creates a modulation that runs perpendicular to the polar axis. If $f_m$ is an integer multiple of $\sigma$, then the modulation runs around the polar axis. If the curve is a single Clelia curve and $f_m = n\sigma + m\ell$, then the modulation pattern matches the Clelia curve $\{m\}\{-n\}$. A smooth modulation is obtained with a raised-cosine interpolation function $I_{cos}(t) = \frac{1 - \cos(2\pi f_m t)}{2}$. $I_{cos}(t)$ is useful for coloring the curve. Another useful interpolation function is a pulse wave

$$
I_{pulse}(t) = \begin{cases} P_1 & \mathrm{frac}(f_m t + \theta_m) \leq w \\ P_2 & \mathrm{frac}(f_m t + \theta_m) > w \end{cases}
\tag{25}
$$

where $w \in [0, 1]$ is the pulse width and $\mathrm{frac}(x) := x - \lfloor x \rfloor$. The pulse wave is particularly effective when applied to the radius of a tube-rendered curve. Pulse modulation between a non-zero and zero radius produces a variety of cutting effects. For $f_m$ an integer multiple of $\ell$ or $\sigma$, sections are cut along parallel (Figure 18b) or meridional (Figure 18c) planes. As indicated above, if $f_m$ is a linear combination of $\sigma$ and $\ell$, then a cutting pattern shaped like a Clelia curve emerges (Figure 18d). Large pulse widths are useful for adding slight imperfections to the curve (Figure 18e). Figure 19 presents an assortment of curves enhanced by both pulse wave cutting and color modulation.
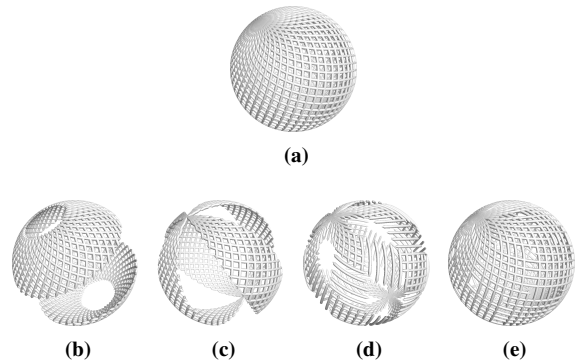


**(a)**

**(b)**     **(c)**     **(d)**     **(e)**

**Figure 18:** Pulse wave cutting applied to a Clelia curve $\{\sigma\}\{\ell\}$ with $\sigma = 40, \ell = 41$: **(a)** uncut curve, **(b)** $f_m = 4\ell, w = \frac{1}{2}, \theta_m = \frac{3}{4}$, **(c)** $f_m = 4\sigma, w = \frac{1}{2}, \theta_m = \frac{3}{4}$, **(d)** $f_m = 5\sigma + 3\ell, w = \frac{1}{2}, \theta_m = 0$ and **(e)** $f_m = 64, w = \frac{9}{10}, \theta_m = 0$.

To modulate between several properties, barycentric coordinates may be used. Letting the properties be the vertices of the simplex, then a barycentric coordinate specifies a weighted sum of all properties where the sum of weights is 1. A convenient way to generate a barycentric coordinate is to square each component of a point lying on a unit $n$-sphere. For three properties, $P_1, P_2, P_3$, we can employ a Clelia curve. A convenient choice is $\{f_{12}/2\}\{f_{13}/2, \frac{1}{4}\}$ where $f_{12}$ and $f_{13}$ are modulation frequencies between $P_1, P_2$ and $P_1, P_3$, respectively.
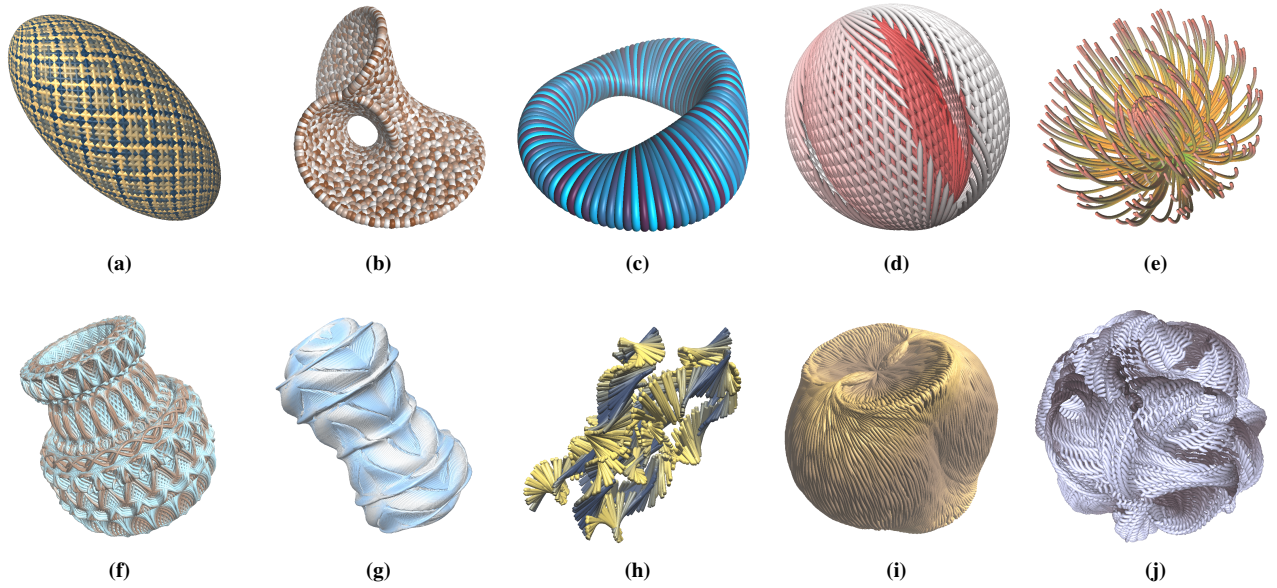
**Figure 19:** Examples of property modulation of curves. For all curves, $f_C$ is the color modulation frequency using the function $I_{cos}$ and, where specified, $f_r$, $\theta_r$ and $w_r$ are the frequency, phase and pulse width of the tube radius modulation using the function $I_{pulse}$.
**(a)** Ellipsoidal curve $\{\sigma\}\{-\ell\} + \frac{1}{3}\{\sigma\}\{\ell\}$ with $\sigma = 101, \ell = 58, f_C = 24\sigma - 40\ell$,
**(b)** twisted ribbon curve $\{\sigma\}\{-\ell\} + \{\sigma\}\{2\sigma + \ell\} + \{\sigma\}\{0, \frac{1}{4}\}$ with $\sigma = 21, \ell = 37, f_C = 1757$ and rendered with $N = 4000$ spheres,
**(c)** twisted torus curve $\{\sigma\}\{-\ell\} + \frac{1}{3}\{\sigma\}\{2\sigma + \ell\} + 3\{\sigma\}\{0, \frac{1}{4}\}$ with $\sigma = 1, \ell = 118, f_C = -53\sigma + \ell$,
**(d)** parallel sweep surface $\{3\sigma\}\{\ell\} + \frac{2}{5}\{\sigma\}\{\ell\}$ with $\sigma = 33, \ell = 200, f_C = 2\sigma, f_r = 11\sigma + \ell, w_r = 0.7$,
**(e)** $\{\sigma\}\{-6\ell\} + \{\sigma\}\{7\ell\} + 2\{\sigma\}\{13\ell\}$ with $\sigma = 1, \ell = 13, f_C = 13\ell, f_r = 13\ell, \theta_r = 0.8, w_r = 0.6$,
**(f)** $\{\sigma + \ell\}\{\ell\} - 0.43\{\sigma\}\{-5\ell\} + 0.06\{-20\sigma\}\{28\ell\}$ with $\sigma = 213, \ell = 215, f_C = -21\sigma + 21\ell$,
**(g)** $\{\sigma + \ell\}\{\ell\} + 0.41\{\sigma + 3\ell\}\{\ell\} - 0.07\{-2\sigma + 12\ell\}\{-13\ell\}$ with $\sigma = 213, \ell = 215, f_C = -6\sigma + 6\ell, f_r = -10\sigma + 19\ell, w_r = 0.9$,
**(h)** $\{2\}\{7\} + \{3\}\{-6\} + \frac{1}{5}\{\sigma\}\{-40\ell\} + \frac{1}{5}\{\sigma\}\{41\ell\}$ with $\sigma = 26, \ell = 29, f_C = \ell, f_r = 13\ell, w_r = 0.6$,
**(i)** $\{\sigma\}\{\ell\} - 0.25\{3\sigma\}\{3\ell\} - 0.01\{8\sigma + 6\ell\}\{17\sigma + 22\ell\}$ with $\sigma = 1, \ell = 200, f_C = 4\ell, f_r = -65\sigma + 2\ell, w_r = 0.9$ and
**(j)** $\{\sigma\}\{\ell\} + 0.25\{-\sigma + 3\ell\}\{4\sigma + 3\ell\} + 0.02\{\sigma + 32\ell\}\{-20\sigma + 50\ell\}$ with $\sigma = 1, \ell = 200, f_C = 3\sigma + 6\ell, f_r = -6\sigma + 2\ell, w_r = 0.85$.

## 12.3. Feature Mapping

Since the components of a Clelia curve are Fourier series, there are several pieces of geometric information that can be extracted from merely the position $t \in [0, 1)$ along the curve. Not only is this information purely local, but it is also exact (up to numerical errors). This stems from the fact that exact derivatives may be obtained for any curve through a combination of (4) and the linearity of differentiation. From (24), we may obtain a rather substantial feature vector of derived geometric information that can be used to enhance the curve, namely through modification of its material properties. A useful strategy is to consider the level sets of scalar functions derived from the feature vector. A level set may be defined through the delta function

$$L_c(x) = \begin{cases} x = c & 1 \\ x \neq c & 0 \end{cases} \qquad (26)$$

where $c$ is the level and the output values indicate membership in the set. In practice, it is helpful to generalize the shape of (26) to a peak with variable spread around the level. Some simple polynomial functions include a triangle window $L_{c,w}(x, w) =$

$\max(0, 1 - |(x - c)/w|)$ and parabolic window $L_{c,w}(x) = \max(0, 1 - ((x - c)/w)^2)$ where $L_{c,w}(c) = 1$ and $L_{c,w}(x) = 0$ for $|x - c| > w$. For a more diffusive style, one may use the Lorentzian function $L_{c,w}(x, w) = w^2/(x^2 + w^2)$ where $L_{c,w}(c) = 1$ and $L_{c,w}(c \pm w) = \frac{1}{2}$. Figure 20 shows several curves with colors derived directly from spread levels sets of curvature and torsion using a Lorentzian function. Each curve consists of a low-amplitude, high-frequency component that imparts only minor spatial displacement, however creates interesting modulations of curvature and torsion along the curve.

## 13. Future Work

One promising direction is to consider generation of spatiotemporal forms using our algorithm. Several families of curves develop according to a generatrix undergoing repetition of basic motions such rotation and scaling. If these basic motions are recast from spatial to temporal motion, then a variety of animation possibilities emerge. It is likely that sensible animation will require further constraints. However, it is intriguing, and perhaps useful, to unify generation of spatial and temporal structure through the same
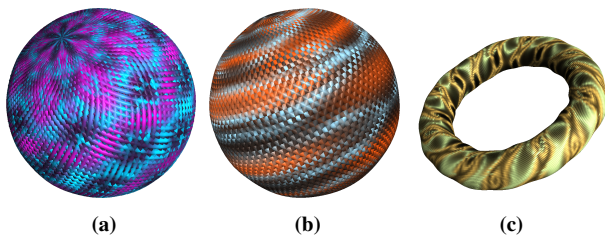
**Figure 20:** *Curves colored according to level sets of curvature and torsion: (a)* $\{\sigma\}\{\ell\} + \frac{4}{1000}\{8\sigma\}\{10\ell\}$ *with* $\sigma = 71, \ell = 81$ *and isocoloring at* $\kappa = 1.6$ *(violet) and* $\tau = 0.5$ *(cyan), (b)* $\{\sigma\}\{\ell\} + \frac{6}{1000}\{3\sigma\}\{10\ell\}$ *with* $\sigma = 71, \ell = 81$ *and isocoloring at* $\kappa = 1.4$ *(orange) and* $\tau = 2.14$ *(sky blue), (c)* $\{\sigma\}\{0, \frac{1}{4}\} + \frac{1}{5}\{\sigma\}\{-2\sigma + \ell\} + \frac{17}{1000}\{13\sigma\}\{2\ell\}$ *with* $\sigma = 80, \ell = 91$ *and isocoloring at* $\kappa = 1$ *(mustard) and* $\tau = 0.9$ *(olive).*

mathematical framework. Another future avenue may be surveying the repertoire of shapes that resemble natural forms such as starfish (Figure 10c), flowers (Figure 19e), pollen grains (Figure 19i) and squashes (Figure 6a) and comparing them to other approaches such as the (3D) superformula [Gie03, GBB03]. Finally, it may be worth exploring applications in 3D printing as shapes with coiled windings ($\ell = 1$, $\sigma$ large as in Figures 7a and 16b) would seem highly amenable to fused filament fabrication processes.

## 14. Conclusion

The sum of Clelia shape generation algorithm is simple, yet produces a wide breadth of outputs from basic to complex. One attribute of the algorithm is that changing its parameters directly often leads to surprising or unexpected results. In general, this uncertainty is an asset, however there are situations where more predictable behavior is desirable such as when procedurally generating shapes. This is addressed with a reparameterized 'envelope form' of the fundamental equation that permits more control over the structure of the curve such as its winding pattern and envelope. The envelope form compactly describes many of the most structured shapes we discovered through experimentation. There are hints that the envelope form describes more families of shapes than outlined here, especially those having $K > 2$ components and non-zero values of $f_k$. From our experimentation, we found $K = 3$ to be a sufficient threshold for producing complex shapes. This is not to suggest that nothing of interest lies beyond this threshold, however, at some point hand-tuning parameters becomes more difficult so more ways to abstract the parameter space may be necessary. We consider the work presented here to be a first step towards gathering a more complete picture of the space of possible forms generated by linear combinations of Clelia curves.

## Acknowledgements

## References

[Ad80] ABELSON H., DISESSA A. A.: *Turtle Geometry: The Computer as a Medium for Exploring Mathematics*. MIT Press, Cambridge, MA, 1980. 1, 2

[Baz75] BAZLEY T. S.: *Index to the Geometric Chuck: A Treatise Upon the Description, In the Lathe, of Simple and Compound Epitrochoidal or "Geometric" Curves*. Waterlow and Sons, London, 1875. 1

[BEEH98] BREIDBACH O., EIBL-EIBERSFELDT I., HARTMANN R.: *Art Forms in Nature: Prints of Ernst Haekel*. Prestel, 1998. 1

[Bis75] BISHOP R. L.: There is more than one way to frame a curve. *American Mathematical Monthly 82*, 3 (1975), 246–251. 10

[Bro07] BROWNE C.: Harmonograms. *Computers and Graphics 31*, 2 (2007), 292–300. 1

[Cha15] CHAPPELL D.: Sinuous meander patterns: a family of multi-frequency spatial rhythms. *Journal of Mathematics and the Arts 9*, 3-4 (2015), 63–76. 1

[Far96] FARRIS F. A.: Wheels on wheels on wheels-surprising symmetry. *Mathematics Magazine 69* (1996), 185–189. 3

[Fra76] FRANKE H. W.: *Artist and Computer*. Harmony Books, New York, 1976, ch. Graphic Music, pp. 21–22. 1

[Fra89] FRANKE H. W.: Mathematics as an artistic-generative principle. *Leonardo 22*, Supplement (1989), 25–26. 1

[Fre52] FRENET J. F.: Sur les courbes à double courbure. *Journal de Mathématiques Pures et Appliquées 17* (1852), 437–447. 10

[Gai05] GAILIUNAS P.: Meanders. In *Renaissance Banff: Mathematics, Music, Art, Culture* (Southwestern College, Winfield, Kansas, 2005), Bridges Conference, pp. 25–30. 1

[GAS06] GRAY A., ABBENA E., SALAMON S.: *Modern Differential Geometry of Curves and Surfaces with Mathematica*. Chapman and Hall/CRC, Boca Raton, FL, 2006. 8

[GBB03] GIELIS J., BEIRINCKX B., BASTIAENS E.: Superquadrics with rational and irrational symmetry. In *Proceedings of the Eighth ACM Symposium on Solid Modeling and Applications* (New York, NY, USA, 2003), ACM, pp. 262–265. 2, 12

[GBKW09] GOOLD J., BENHAM C. E., KERR R., WILBERFORCE L. R.: *Harmonic Vibrations and Vibration Figures*. Newton and Co., London, 1909. 1

[GdW16] GOEMANS W., DE WOESTYNE I. V.: Twisted surfaces with null rotation axis in minkowski 3-space. *Results in Mathematics 70*, 1 (2016), 81–93. 2

[Gie03] GIELIS J.: A generic geometric transformation that unifies a wide range of natural abstract shapes. *American Journal of Botany 90*, 3 (2003), 333–338. 1, 12

[Gla97] GLASSNER A. S.: A shape synthesizer. *IEEE Computer Graphics and Applications 17*, 3 (1997), 40–51. 1

[Gra28] GRANDI G.: *Flores Geometrici ex Rhodonearum, et Cloeliarum Curvarum Descriptione Resultanates*. Typis Regiae Celsitudinis, Florentiae, 1728. 2

[HM95] HANSON A. J., MA H.: *Parallel Transport Approach to Curve Framing*. Tech. Rep. TR425, Indiana University, School of Informatics and Computing, 1995. 10

[Hof79] HOFSTADTER D. R.: *Gödel, Escher, Bach: An Eternal Golden Braid*. Vintage Books, New York, 1979. 6

[ID33] IBBETSON J. H., DIBNER B.: *A Brief Account of Ibbetson's Geometric Chuck, Manufactured by Holtzapffel and Co.: With a Selection of Specimens Illustrative of Some of Its Powers*. A. Hancock, London, 1833. 1

[Kaw82] KAWAGUCHI Y.: A morphological study of the form of nature. In *SIGGRAPH 1982 Conference Proceedings* (New York, 1982), ACM, pp. 223–232. 1

[KI15] KRIVOSHAPKO S., IVANOV V.: *Encyclopedia of Analytical Surfaces*. Springer International Publishing, Switzerland, 2015. 4, 5

[Lap53] LAPOSKY B.: *Electronic Abstractions: A New Approach to Design*. Ben Laposky, Cherokee, IA, 1953. 1

[Lap69] LAPOSKY B.: Oscillons: Electronic abstractions. *Leonardo 2*, 4 (1969), 345–354. 1, 10

[Lis57] LISSAJOUS J. A.: Mémoire sur l'étude optique des mouvements vibratoires. *Annales de Chimie et de Physique 51* (1857), 147–231. 2

[Man82] MANDELBROT B. B.: *The Fractal Geometry of Nature*. W. H. Freeman and Co., New York, 1982. 1

[Mar74] MAREY É.-J.: *Animal Mechanism: A Treatise on Terrestrial and Aerial Locomotion*. D. Appleton and Company, New York, 1874. 1

[Mar95] MAREY É.-J.: *Movement*. William Heinemann, London, 1895. 1

[MBD*14] MCCORMACK J., BOWN O., DORIN A., MCCABE J., MONRO G., WHITELAW M.: Ten questions concerning generative computer art. *Leonardo 47*, 2 (2014), 135–141. 1

[MBDJ04] MCCORMACK J., BIRD J., DORIN A., JONSON A.: *Impossible Nature: The Art of Jon McCormack*. Australian Centre for the Moving Image, Melbourne, Australia, 2004. 1

[Mon50] MONGE G.: *Application de l'analyse a la gèomètrie*. Bachelier, Paris, 1850. 9, 10

[MP98] MONRO G., PRESSING J.: Sound visualization using embedding: The art and science of auditory autocorrelation. *Computer Music Journal 22*, 2 (1998), 20–34. 2

[Nor68] NORTHCOTT W. H.: *A Treatise on Lathes And Turning, Simple, Mechanical, And Ornamental*. Longmans, Green, and Company, London, 1868. 4

[OTB*17] ORGEMAN K., TURRELL J., BORGEN M., DEBLOCK J., SNOW C., ZINMAN G.: *Lumia: Thomas Wilfred and the Art of Light*. Yale University Art Gallery, New Haven, 2017. 10

[Pap72] PAPERT S.: Teaching children to be mathematicians vs. teaching children mathematics. *International Journal of Mathematical Education and Sciences 3*, 3 (1972), 249–262. 1

[PL90] PRUSINKIEWICZ P., LINDENMAYER A.: *The Algorithmic Beauty of Plants*. Springer-Verlag, New York, 1990. 1

[Put12] PUTNAM L.: *The Harmonic Pattern Function: A Mathematical Model Integrating Synthesis of Sound and Graphical Patterns*. PhD thesis, University of California, Santa Barbara, 2012. 3

[Put14] PUTNAM L.: A method of timbre-shape synthesis based on summation of spherical curves. In *Proceedings of the 40th International Computer Music Conference and 11th Sound and Music Computing Conference* (Athens, Greece, 2014), National and Kapodistrian University of Athens, pp. 1332–1337. 2

[Rig26] RIGGE W. F.: *Harmonic Curves*. Loyola University Press, Chicago, Illinois, 1926. 1

[Rim12] RIMINGTON A. W.: *Colour-Music: The Art Of Mobile Colour*. Hutchinson and Co., London, 1912. 10

[Rob94] ROBERT A.: Fourier series of polygons. *The American Mathematical Monthly 101*, 5 (1994), 420–428. 4

[Ser51] SERRET J. A.: Sur quelques formules relatives à la théorie des courbes à double courbure. *Journal de Mathématiques Pures et Appliquées 16* (1851), 193–207. 10

[TL92] TODD S., LATHAM W.: *Evolutionary Art and Computers*. Academic Press, London, 1992. 1, 2

[Wag70] WAGLER S. R.: Sonovision: A visual display of sound. *Leonardo 3*, 4 (1970), 443–445. 2

[Whi80] WHITNEY J.: *Digital Harmony: On the Complementarity of Music and Visual Art*. Byte Books, Peterborough, NH, 1980. 1

[Wol02] WOLFRAM S.: *A New Kind of Science*. Wolfram Media, Inc., Champaign, IL, 2002. 1